



Article

Host–Virus Interactions in Japanese Encephalitis Virus

Urmi Roy

Department of Chemistry & Biomolecular Science, Clarkson University, 8 Clarkson Avenue, Potsdam, NY 13699-5820, USA; urmi@clarkson.edu

Abstract: Japanese encephalitis (JE) is a mosquito-borne zoonotic disease that causes severe brain inflammation. The JE virus envelope protein domain III (JEV-ED3) plays a critical role in activating receptor binding and membrane fusion. This communication briefly describes, in a computational approach, how structural changes within the JEV-ED3 mutant epitopes suppress their antibody neutralization function. The simulated results demonstrate that mutant Ser40Lys acts as an antibody neutralization escape while Asp41Arg may play the role of an escape mutant. Additionally, an examination of the double mutants on JEV-ED3 suggests that these mutants may qualify as stronger neutralizing escape agents than their single variants. The structural analysis of this work helps to identify the proper antiviral target sequences and specific monoclonal antibodies for the JEV-ED3 escape mutants.

Keywords: escape mutation; host–virus interaction; Japanese encephalitis virus; structural modeling



Citation: Roy, U. Host–Virus Interactions in Japanese Encephalitis Virus. *Zoonotic Dis.* **2022**, *2*, 117–125. <https://doi.org/10.3390/zoonoticdis2030012>

Academic Editor: Stephen K. Wikel

Received: 9 July 2022

Accepted: 3 August 2022

Published: 5 August 2022

Publisher's Note: MDPI stays neutral with regard to jurisdictional claims in published maps and institutional affiliations.



Copyright: © 2022 by the author. Licensee MDPI, Basel, Switzerland. This article is an open access article distributed under the terms and conditions of the Creative Commons Attribution (CC BY) license (<https://creativecommons.org/licenses/by/4.0/>).

1. Introduction

Computational Structural Immunology is an active field where immuno-informatics tools and databases are used to predict antibody structures as well as vaccine candidates. Such structure-based predictions can help to evaluate/identify host–pathogen interactions and epitopes [1–3]. Molecular level analyses of host–virus interactions and identification of antibody neutralizing escape mutations are particularly important under the current clinical challenges linked to the global SARS-CoV-2 crisis and to combating recently emerged zoonoses [4,5].

Zoonoses or zoonotic diseases are triggered by pathogens and are transmitted from animal to human hosts. Common examples of zoonotic diseases are Japanese encephalitis, Lyme disease, monkey pox, plague, rabies, tick-borne diseases, west Nile, zoonotic influenzas and the recently emerged SARS-CoV-2 [6–11]. Japanese encephalitis (JE) is a *Culex* mosquito-borne zoonotic disease that causes severe brain inflammation and is mostly found in Asia [12]. Every year, the JE virus (JEV) infects around 68,000 people, resulting in nearly 13,000 to 20,000 deaths worldwide [13]. JEV belongs to the *Flaviviridae* family, which also includes dengue, St. Louis encephalitis, tick-borne, west Nile and zika viruses. The JEV envelope protein domain III (JEV-ED3) plays a critical role in activating receptor binding and membrane fusion. The outer boundary of the JEV-ED3 harbors the functional epitopes responsible for antibody (Ab) neutralization [14–18]. In this communication, we briefly describe how structural changes within the mutant epitopes suppress their antibody neutralization function. Specifically, we examine the mutated ED3 residues that lose contact with the fragment antigen binding (Fab) region of monoclonal Ab (mAb). This work is an extension of our previous report on a related topic [16].

2. Materials and Methods

We consider the protein databank structure, 1PJW as wild type (wt) Beijing-1 strain structure of JEV-ED3 [19]. The predominant Ab-neutralizing escape mutations identified on JEV-ED3 are Ser330 and Asp331, which correspond to the 1PJW residues 40 and 41,

respectively. These mutant residues were selected based on the experimental work reported by Lin and Wu [14]. Docking simulations using GrammX server were performed to identify the host (mAb-Fab)-virus (JEV-ED3) interactions [20,21]. Repeatability of the JEV-ED3/mAb-Fab complex formation was verified by employing another docking program, “Patch dock”, where docking was performed in the framework of molecular shape recognition [22,23]. Subsequently, the docked structures were further refined by the “Fire dock” server [24,25].

In view of the lack of readily available mAb E3.3 structures, we selected the model 1A3R.PDB (Fab-8F5) as mAb [26] on the basis of previously reported considerations [14].

In that work, the designed model of mAb E3.3 was based on the 1A3R structure. 1A3R.PDB is the X-ray crystal structure of antibody Fab fragment, mAb 8F5, complexed with the peptide of viral capsid protein from human rhinovirus. Given the significance of ED3 epitopes for the antibody neutralization process, and considering 8F5 as a neutralizing Ab for human rhinovirus 2, the Fab-8F5 structure was selected in this experiment as a model for mAb structure. Here, the 1A3R was truncated, and the viral peptide was removed. 1A3R has more than 80% sequence identities with Zika- and dengue-ED3-bound Fabs. Four separate docking simulations were performed using the wt ligand, ligand with single mutations (mutant1, Ser40Lys or mutant2, Asp41Arg) and the ligand with double mutations (Ser40Lys and Asp41Arg) of JEV-ED3. Molecular dynamics simulations were executed for JEV-ED3 bound 1A3R to determine the structural stability of the wt and mutant residues. NAMD, QwikMD and VMD software systems were used for simulations [27–29], with the incorporation of the implicit solvation method, employing the Generalized Born implicit solvent (GBIS) models [30].

For implicit solvent parameters, the alpha cutoff and the ion concentration were set at 14.0 Å and 0.15 mol/L, respectively. For the simulations, protein structure files (.PSF) were initially generated, and energy minimization was performed for 2000 steps. Annealing was performed for 0.24 ns with a gradual ramp of temperature increase from 60 to 300 K. Equilibration was performed for 0.40 ns. After initial minimization, annealing and equilibration, the final production run was executed for 20 ns in the NVT ensemble using Langevin dynamics at a temperature of 300 K. Langevin damping was set to 1, and Langevin piston was set to off.

For the simulations, the integration time step was set to 2 fs, and the CHARMM36 force field was employed [31]. Short-range non-bonded and long-range electrostatics interactions were updated using the reversible reference system propagation algorithm (r-RESPA) of multiple time steps pattern [27]. The non-bonded frequency and the electrostatic frequency were set to the values of 1 and 2 units, respectively. For annealing and equilibration protocols, the backbones were restrained, while no atoms were constrained during the final MD run. Most of these above parameters were available from the NAMD default setting [27]. Additional details of the simulation procedure have been described elsewhere [32–34]. The figures were generated using BIOVIA Discovery Studio Visualizer [35].

3. Results and Discussions

Figure 1A displays a schematic drawing of mAb. The detectable bindings of the wt JEV-ED3 units to mAb-Fab are displayed in Figure 1B. Figure 1B shows a model of wtJEV-mAb, where the wt residues Ser 40 and Asp 41 reside within 3.5 Å (a reference “proximity” chosen for our simulation) from the mAb Fab. In the case of wt Ser40, the inter-chain H-bonds, (H: Ala53) and (H: Tyr33), are observed at the 1PJW-1A3R complex, where numerous inter-chain *van der Waals* interactions are detected. In wt Asp41, a small bump, most likely caused by close residue-contacts and torsional strains, is observed between A:Asp41 and H:Ala53. Usually, these small bumps disappear during the refinement processes of the simulation. A scheme of these interactions is displayed in Figure 1C,D.

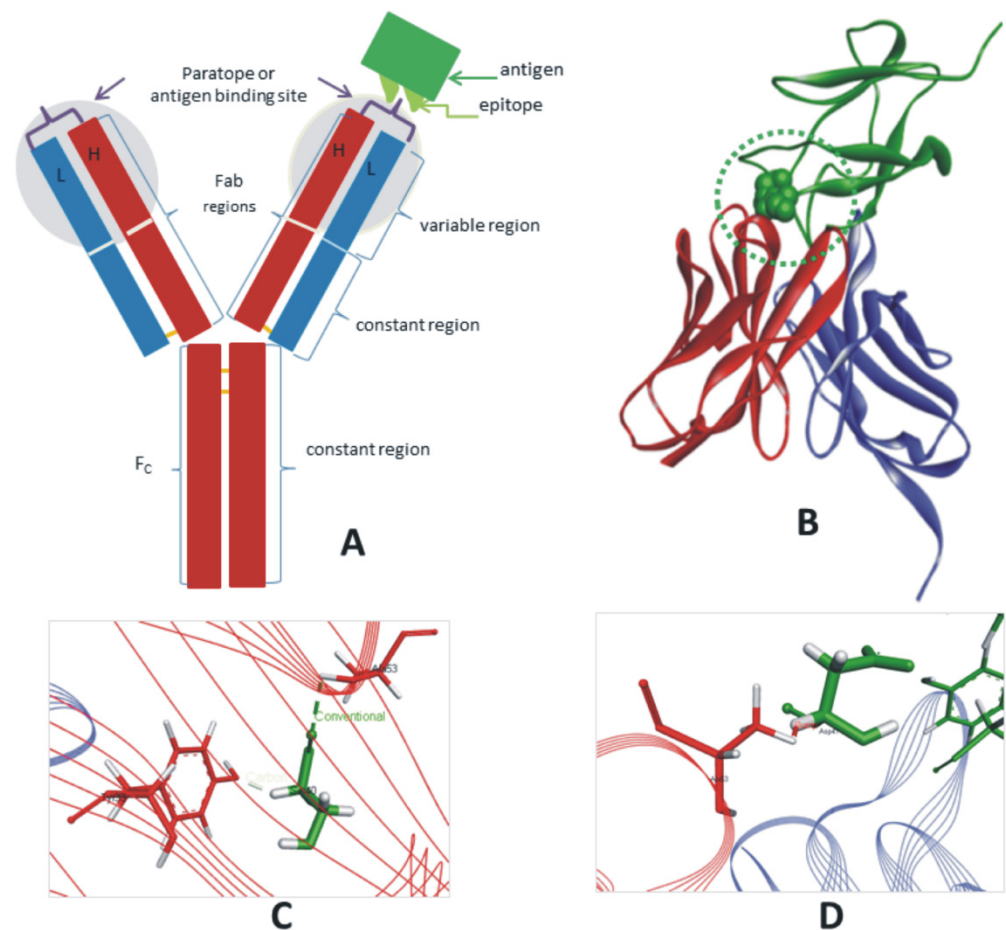


Figure 1. (A) Schematic representation of an antibody structure, where H and L denote the heavy (red) and light (blue) chains, respectively. Antigen is colored in green. (B) Predicted immune-complex of wt JEV-ED3 (1PJW, green) and Fab variable regions (truncated 1A3R). The wt Ser40 and wt Asp41 residues are displayed in green CPK. The mAb-Fab heavy and light chains are colored in red and blue ribbons, respectively. (C,D) Residue interactions in 1PJW-1A3R complex. Only inter-chain interactions are displayed. (C) The wt Ser40 interactions with mAb in 1PJW-1A3R complex. (D) The wt Asp41 residue interactions with mAb in 1PJW-1A3R complex.

In the mutant1-mAb system, the mutant residue Lys40 did not exhibit its expected binding to mAb. The representations of mutant1 ligand protein in Figure 2A1,A2 are near the Fab-8F5 paratope. Mutant Lys40 on the mutated ED3 loses contacts with its neighboring mAb-Fab, and does not have inter-chain H bonds or the vdW interactions. Additionally, since mutant Lys40 no longer resides within 3.5 Å from the Ab, it is likely that Lys40 promotes neutralization escape.

In the mutant2-mAb interactions, most mutant2 models do not bind properly to the mAb-Fab. Figure 2B1,B2 represent the postures of mutant2 JEV-ED3 close to that of Fab-paratope. In both cases, Arg41 resides within 3.5 Å from mAb. No inter-chain interactions are observed between mutant Arg41 and Fab-8F5 in the model presented in Figure 2B1. In Figure 2B2, aside from the presence of a bump, an inter-chain alkyl interaction is identified between Arg41 and Fab: H Ala53. Despite being hydrophobic, the alanine surface is exposed here, and the alkyl side chains of Ala on such an exposed surface may act to destabilize the protein complex. Owing to its unfavorable interactions, Arg41 may serve as an Ab neutralization escape mutant. For the purpose of simulation, we have selected the mutant2 complex displayed in Figure 2B2. Based on these models, the Lys40 appears to be an Ab neutralization escape mutant, while Arg41 may also be effective as an Ab neutralization escape mutant.

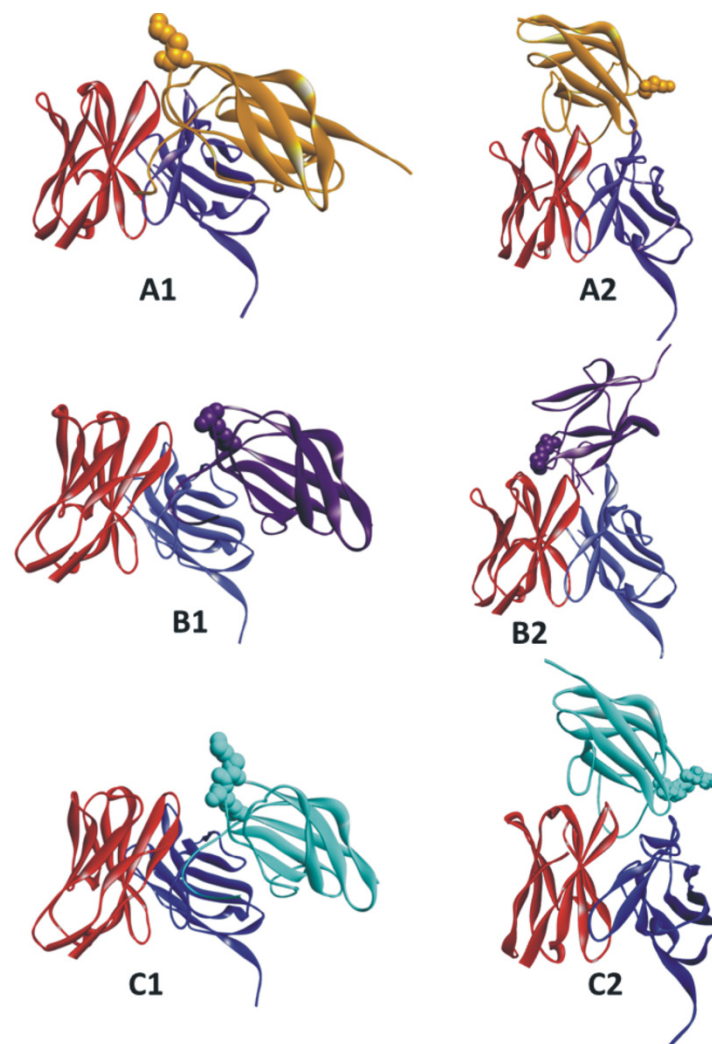


Figure 2. Predicted interactions between mutant JEV-ED3 and mAb-Fab variable regions (truncated 1A3R). The Fab heavy and light chains are colored in red and blue, respectively. (A1,A2) Predicted complexes of mutant1 ligand protein (orange) and Fab receptor. Mutant Lys40 residue is displayed in orange CPK. (B1,B2) Predicted complexes of mutant2 ligand protein (violet) and Fab receptor. Mutant Arg41 residue is displayed in violet CPK. (C1,C2) Predicted complexes of double-mutant ligand protein (cyan) and Fab receptor. Here, the mutant residues Lys40 and Arg41 are displayed in cyan CPK.

For the double-mutant–mAb complex (Figure 2C1), the mutant residues do not interact with mAb (Figure 3A,B). In the model from Figure 2C2, the mutant Lys40 is not located within the reference proximity of 3.5 Å from Fab-8F5, and does not have any inter-chain interactions (Figure 3C). However, Arg 41 is located within this proximity from 1A3R, and experiences positive–positive repelling interactions with mAb L: Lys30 (Figure 3D). These repulsion forces can lead to mutant Arg41 acting as an escape mutant.

The detailed interactions between the double-mutant JEV-ED3 and mAb are displayed in Figure 3. Since the first model of the double-mutant complex (Figure 2C1) does not have any inter-chain interactions, the second model (Figure 2C2) is chosen for MD simulation. Some inter-chain steric clashes are observed in mutant Arg41 (Figures 2C2 and 3D); the initially observed bumps eventually disappeared during the refinement and simulation processes. Based on this observation, it is expected that the Arg41 in the other complex (Figures 2C1 and 3B) also follow the same trend. Nonetheless, JEV-ED3 mutant epitopes are not completely understood at this time, since some of them do not manifest decreased antibody cross-reactivity [36].

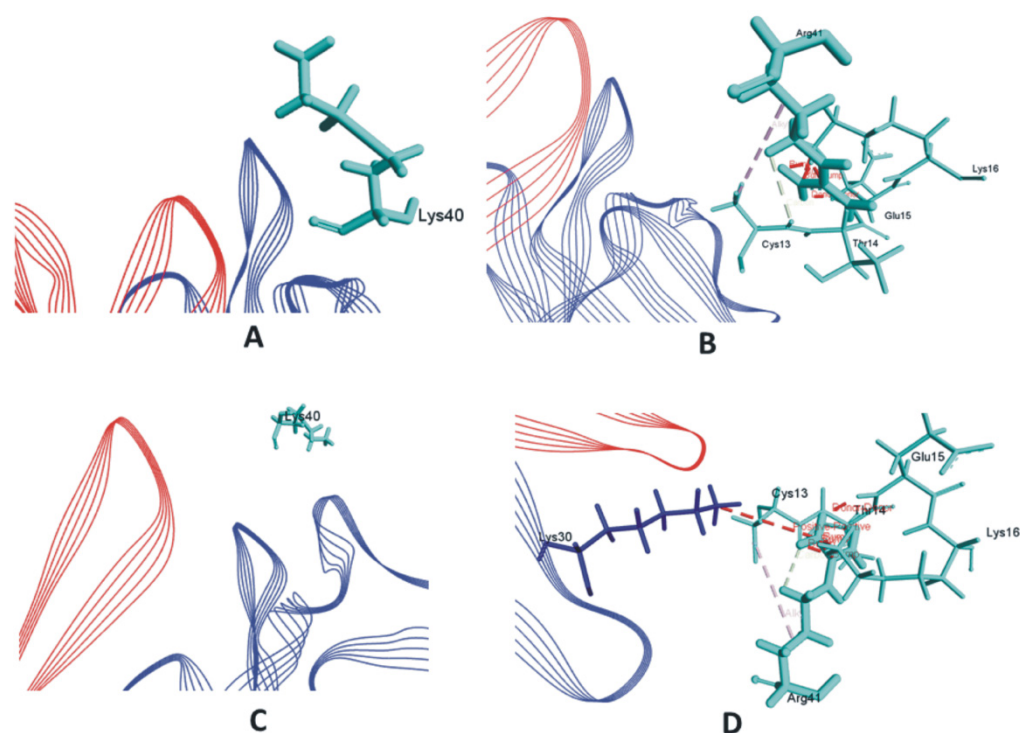


Figure 3. Tentative interactions within the double-mutant JEV-ED3/mAb-Fab complex. (A) Interactions between mutant Lys40 JEV-ED3/mAb within the double-mutant complex. (B) Interactions between mutant Arg41 JEV-ED3/mAb within the double-mutant complex. The interactions shown in (A,B) are based on double-mutant JEV-ED3/mAb-Fab displayed in Figure 2C1. (C) Interactions between mutant Lys40 JEV-ED3/mAb within the double-mutant complex. (D) Interactions between mutant Arg41 JEV/mAb within the double-mutant complex. The interactions shown in (C,D) are based on double-mutant/mAb-Fab complex displayed in Figure 2C2.

Although the Chimpanzee mAb-Fabs show some effectivity against this virus, the antibody neutralizing escape mutants continue to pose challenges for understanding their detailed behavior [18].

To check repeatability of the complex formation, we have performed an additional docking simulation using “Patchdock”. Here, the docked structures were further refined by the “Firedock” server, where the binding energy values of the solution were readily accessible [22–25]. The predicted docked models of wt and mutant variants were selected from the first twenty filtered best scoring structures. Visual inspection plays a crucial role in selecting the docked complexes. These complexes are presented in Supplementary Figure S1.

Referring to the Supplementary section, Figure S1A displays the wt JEV-ED3/mAb-Fab complex; for visual inspection, this is the most suitable ligand binding mode out of the first twenty refined structures, and it has a global energy of -20.64 energy unit. In the case of mutant1-mAb, most of the mutant1 ligand did not bind to a proper (stabilizing) region of mAb. The mutant2-mAb complex, characterized by with an energy value of -9.49 energy unit, is depicted in Figure S1B. The double-mutant JEV-ED3/mAb-Fab complexes, is displayed in Figure S1C, and is characterized by global energy value of -8.39 energy unit, respectively.

The global energy value for the wt protein complex is lower than those of mutant-2 and the double-mutant complex, although these values may change during the course of a simulation. Therefore, based on the results of the second docking, it is reasonable to conclude that these findings are fairly consistent with the first docking experiments, that the wt protein forms a stable complex with mAb-Fab, and that these mutations may be linked to antibody neutralization escape.

The combined results of the two foregoing experiments are indicative of the overall efficacy of docked complex formation. It is also useful to emphasize that blind docking was performed in this study, with no constrained interfacial residues. Nonetheless, it should be noted in this context that in all the above cases, docked structures exist where the wt or mutant ligand protein did not bind to the paratope region of the mAb, and those models are not considered in the present context. The exclusion of the model structures where interactions between residues 40 and 41 with mAb were absent may divert the formation of expected structures of mutant Ag/mAb complexes. As both mutations had overall destabilizing effects on the antibody binding region (epitope), it is possible that the preferred mutant Ag/mAb interactions moved to the other regions of the protein.

Figure 4 displays root-mean-square deviations (RMSD) measured during the MD simulation for some of the wt or mutant residues. These calculations excluded those immune complexes for which interactions of the receptor Fab with ligand residues 40 or /and 41 were absent. The wt residues, Ser40 and Asp41, in the wt JEV-ED3/mAb complex (Figure 1B) have lower RMSD values compared to that of Arg41 (in mutant2 JEV-ED3/mAb; model displayed in Figure 2B2) or Lys40 and Asp41 (in double-mutant JEV-ED3/mAb; model displayed in Figure 2C2). Time-based secondary structural changes in the corresponding wt and mutant ligand proteins are displayed in the electronic Supplementary materials Figure S2. According to these results, the double mutant appears to have essentially the same effects of individual single-point mutations, and together, they may qualify as a stronger neutralizing escape agent than in their individual forms.

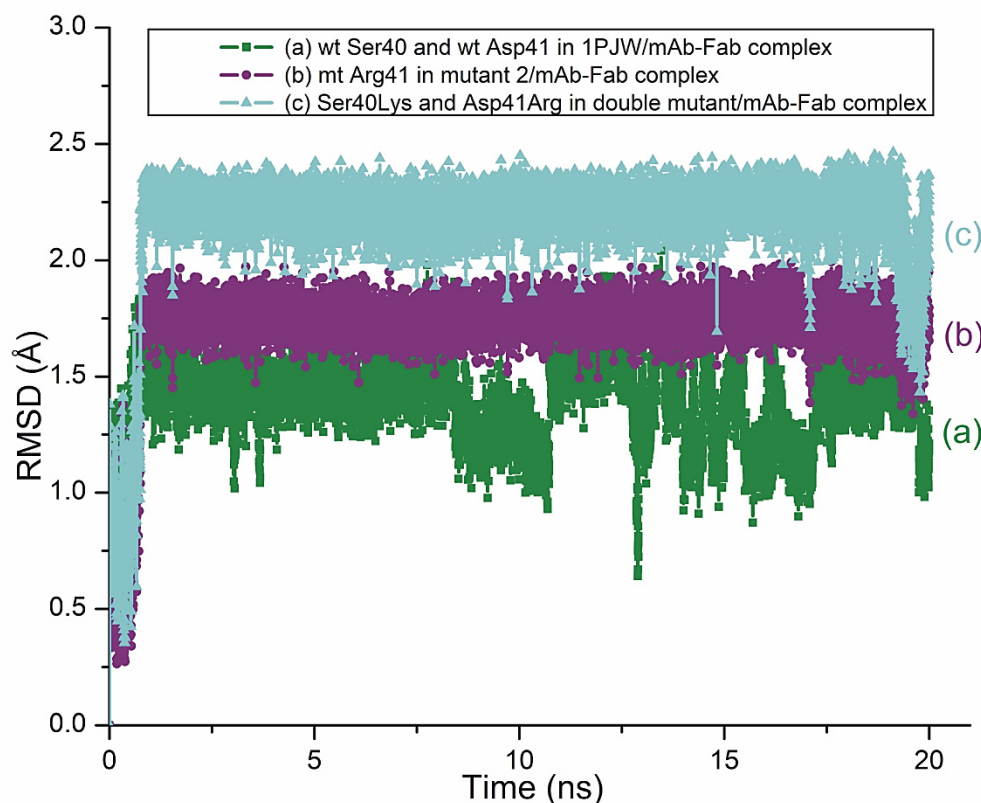


Figure 4. The RMSD variations of wt and mutant ligand residues in JEV-ED3/mAb-Fab complexes. (a) The RMSD plot of wt residues 40 and 41 in JEV-ED3/mAb-Fab complex. This plot refers to the configuration shown in Figure 1B. (b) The RMSD plot of mutant residue 41 in mutant2 JEV-ED3/antibody complex. This plot refers to the configuration shown in Figure 2B2. (c) The RMSD plot of double-mutant residues 40 and 41 in double-mutant JEV-ED3/antibody complex. This plot refers to the configuration shown in Figure 2C2.

We have calculated the binding energies for the wt and mutant ligand–receptor complexes by using structural coordinates corresponding to the time frame at 20 ns ($t = 20$ ns; final trajectory). This time-selected approach helped to minimize the computation time necessary for obtaining binding energy estimates. Energy calculations were performed using the Swiss PDB viewer [37] with Gromos96 [38] implementation. As we discuss below, these calculations yielded negative binding energies necessary to stabilize both the wt and the mutant complexes.

Since the calculated RMSD values of mutant residues 40 and 41 in double-mutant JEV-ED3/antibody complex was higher than those of wt residues 40 and 41 in the wt JEV-ED3/mAb-Fab complex (Figure 4), we have selected the complexes of wt and the double mutant for binding energy calculations considering the possibility that a double mutant might act as more effective antibody neutralization escape than its constituent individual components. For the wt protein the calculated values of the binding energy at $t = 20$ ns was -829.463 KJ/mL. This was the binding energy of the wt JEV-ED3/mAb-Fab receptor complex displayed in Figure 1B. The calculated binding energy value for the double-mutant ligand/receptor complex at 20 ns was found to be -709.234 KJ/mol. This was the binding energy of the double-mutant JEV-ED3/mAb-Fab receptor complex displayed in Figure 2C2. Thus, it is evident that the wt protein complex remains stable throughout the sampling time, as indicated by the negative energy of the complex recorded at the end of sampling.

The results of docking and scoring experiments and ligand–receptor interaction studies demonstrate that mutant Ser40Lys acts as an antibody neutralization escape while Asp41Arg may also play the role of an antibody neutralization escape mutant. Further, the calculated RMSD values reinforce our assessment that the double-mutant variant may function as a better neutralizing escape mutant than its single mutant variants. Additionally, the lower binding energy of the wt species measured at the final simulation state is supportive of our conclusion that the wt protein forms a stable complex with greater mAb binding affinity.

The SARS-CoV-2 pandemic of 2020 has pointedly brought out the implication of viral zoonotic diseases as major public health threats [39,40]. As JEV-RNA viruses are subject to epidemiological fitness and frequent mutational changes, they also have the potential of becoming a significant health hazard under favorable spreading conditions. Therefore, it is useful to fully understand their structural basis, which, through translational research, may help to identify proper therapeutic targets and prevent potential outbreaks of the JEV antibody neutralization escape mutants. The structural results presented in this work contribute an effort aimed in that direction.

Supplementary Materials: The following supporting information can be downloaded at: <https://www.mdpi.com/article/10.3390/zoonoticdis2030012/s1>, Figure S1: The wt and mutant JEV-ED3/mAb-Fab complexes using Pathdock and Firedock server. A. The wt JEV-ED3/receptor complex. The global energy value for this complex is -20.64 energy unit. B. The mutant2 (Asp41Arg)/receptor complex, with global energy value -9.49 energy unit. C. Double-mutant/receptor complex with a different ligand binding mode is displayed. The global energy value for this complex is -8.39 energy unit. These values may change during the simulation process. Figure S2: Secondary structure changes in wt and mutant ligand proteins with time. A. Secondary structure changes in wt 1PJW-ED3 ligand in JEV-ED3/mAb-Fab complex (This plot refers to the configuration shown in Figure 1B of the main article). B. Secondary structure changes in mutant2 ligand protein in mutant2/mAb S6 Fab complex (This plot refers to the configuration shown in Figure 2B2 of the main article). C. Secondary structure changes in double-mutant ligand protein in double-mutant/mAb-Fab complex (this plot refers to the configuration shown in Figure 2C2 of the main article). D. The scheme of the color codes used in this figure is described. Default color codes are used. The X axis represents the frames corresponding to the simulation time. On this scale, the 20 ns correspond to 10,000 frames. The Y axis denotes the proteins' residue numbers.

Funding: This research received no external funding.

Institutional Review Board Statement: Not applicable.

Informed Consent Statement: Not applicable.

Data Availability Statement: The dataset generated during this study is available from the corresponding author upon request.

Acknowledgments: The author acknowledges utilization of the following simulation and visualization software packages: (1) NAMD and (2) VMD: NAMD and VMD, developed by the Theoretical and Computational Biophysics Group in the Beckman Institute for Advanced Science and Technology at the University of Illinois, Urbana-Champaign; (3) Discovery Studio Visualizer: Dassault Systèmes BIOVIA, Discovery Studio Modeling Environment, San Diego, CA: Dassault Systèmes (2015).

Conflicts of Interest: The author declares no conflict of interest.

References

1. Al-Abdulla, O.; Kallström, A.; Valderrama, C.; Kauhanen, J. Simulation of the Progression of the COVID-19 Outbreak in Northwest Syria Using a Basic and Adjusted SIR Model. *Zoonotic Dis.* **2022**, *2*, 44–58. [CrossRef]
2. Moczydlowski, E. Ion Channels. In *Methods in Enzymology*; Rudy, B., Iverson, L., Eds.; Elsevier Inc.: Amsterdam, The Netherlands, 1992; Volume 207, pp. 791–806.
3. Head, J.F.; Swamy, N.; Ray, R. Crystal structure of the complex between actin and human vitamin D-binding protein at 2.5 Å resolution. *Biochemistry* **2002**, *41*, 9015–9020. [CrossRef] [PubMed]
4. Wikel, S. Ticks and tick-borne pathogens at the cutaneous interface: Host defenses, tick countermeasures, and a suitable environment for pathogen establishment. *Front. Microbiol.* **2013**, *4*, 337. [CrossRef] [PubMed]
5. Khayat, R.; Russell, R.S. It is all about the Structure. *Viral Immunol.* **2021**, *34*, 1–2. [CrossRef]
6. Beck, C.; Hamel, R.; Dumarest, M.; Gonzalez, G.; Lecollinet, S. Chapter 42—Nonhuman occurrence of Zika virus infection: Implications for control. In *Zika Virus Biology, Transmission, and Pathology*; Martin, C.R., Martin, C.J.H., Preedy, V.R., Rajendram, R., Eds.; Academic Press: Cambridge, MA, USA, 2021; pp. 453–465.
7. Cáceres, C.J.; Rajao, D.S.; Perez, D.R. Airborne Transmission of Avian Origin H9N2 Influenza A Viruses in Mammals. *Viruses* **2021**, *13*, 1919. [CrossRef]
8. Rupprecht, C.E.; Van Pelt, L.I.; Davis, A.D.; Chipman, R.B.; Bergman, D.L. Use of a Direct, Rapid Immunohistochemical Test for Diagnosis of Rabies Virus in Bats. *Zoonotic Dis.* **2022**, *2*, 1–8. [CrossRef]
9. Talactac, M.R.; Hernandez, E.P.; Hatta, T.; Yoshii, K.; Kusakisako, K.; Tsuji, N.; Tanaka, T. The antiviral immunity of ticks against transmitted viral pathogens. *Dev. Comp. Immunol.* **2021**, *119*, 104012. [CrossRef]
10. Hai, R.; García-Sastre, A.; Swayne, D.E.; Palese, P. A reassortment-incompetent live attenuated influenza virus vaccine for protection against pandemic virus strains. *J. Virol.* **2011**, *85*, 6832–6843. [CrossRef]
11. Yamayoshi, S.; Kawaoka, Y. Emergence of SARS-CoV-2 and its outlook. *Glob. Health Med.* **2020**, *2*, 1–2. [CrossRef]
12. CDC. Centers for Disease Control and Prevention (CDC), Japanese Encephalitis. Available online: <https://www.cdc.gov/japaneseencephalitis/> (accessed on 1 July 2022).
13. WHO. World Health Organization, Japanese Encephalitis. Available online: <https://www.who.int/en/news-room/fact-sheets/detail/japanese-encephalitis> (accessed on 21 May 2022).
14. Lin, C.-W.; Wu, S.-C. A functional epitope determinant on domain III of the Japanese encephalitis virus envelope protein interacted with neutralizing-antibody combining sites. *J. Virol.* **2003**, *77*, 2600–2606. [CrossRef]
15. Luca, V.C.; AbiMansour, J.; Nelson, C.A.; Fremont, D.H. Crystal structure of the Japanese encephalitis virus envelope protein. *J. Virol.* **2012**, *86*, 2337–2346. [CrossRef] [PubMed]
16. Roy, U. Structural and molecular analyses of functional epitopes and escape mutants in Japanese encephalitis virus envelope protein domain III. *Immunol. Res.* **2020**, *68*, 81–89. [CrossRef] [PubMed]
17. Rey, F.A.; Stiasny, K.; Vaney, M.C.; Dellarole, M.; Heinz, F.X. The bright and the dark side of human antibody responses to flaviviruses: Lessons for vaccine design. *EMBO Rep.* **2018**, *19*, 206–224. [CrossRef] [PubMed]
18. Goncalvez, A.P.; Chien, C.H.; Tubthong, K.; Gorshkova, I.; Roll, C.; Donau, O.; Schuck, P.; Yoksan, S.; Wang, S.D.; Purcell, R.H.; et al. Humanized monoclonal antibodies derived from chimpanzee Fabs protect against Japanese encephalitis virus in vitro and in vivo. *J. Virol.* **2008**, *82*, 7009–7021. [CrossRef] [PubMed]
19. Wu, K.P.; Wu, C.W.; Tsao, Y.P.; Kuo, T.W.; Lou, Y.C.; Lin, C.W.; Wu, S.C.; Cheng, J.W. Structural basis of a flavivirus recognized by its neutralizing antibody: Solution structure of the domain III of the Japanese encephalitis virus envelope protein. *J. Biol. Chem.* **2003**, *278*, 46007–46013. [CrossRef]
20. Tovchigrechko, A.; Vakser, I.A. GRAMM-X public web server for protein-protein docking. *Nucleic Acids Res.* **2006**, *34*, W310–W314. [CrossRef]
21. Tovchigrechko, A.; Vakser, I.A. Development and testing of an automated approach to protein docking. *Proteins* **2005**, *60*, 296–301. [CrossRef]
22. Duhovny, D.; Nussinov, R.; Wolfson, H.J. Efficient Unbound Docking of Rigid Molecules. In Proceedings of the 2nd Workshop on Algorithms in Bioinformatics (WABI), Rome, Italy, 17–21 September 2002; Gusfield, E., Ed.; Springer: Berlin/Heidelberg, Germany, 2002; Volume 2452, pp. 185–200.

23. Schneidman-Duhovny, D.; Inbar, Y.; Nussinov, R.; Wolfson, H.J. PatchDock and SymmDock: Servers for rigid and symmetric docking. *Nucleic Acids Res.* **2005**, *33*, W363–W367. [[CrossRef](#)]
24. Andrusier, N.; Nussinov, R.; Wolfson, H.J. FireDock: Fast interaction refinement in molecular docking. *Proteins* **2007**, *69*, 139–159. [[CrossRef](#)] [[PubMed](#)]
25. Mashlach, E.; Schneidman-Duhovny, D.; Andrusier, N.; Nussinov, R.; Wolfson, H.J. FireDock: A web server for fast interaction refinement in molecular docking. *Nucl. Acids Res.* **2008**, *36*, W229–W232. [[CrossRef](#)]
26. Tormo, J.; Blaas, D.; Parry, N.R.; Rowlands, D.; Stuart, D.; Fita, I. Crystal structure of a human rhinovirus neutralizing antibody complexed with a peptide derived from viral capsid protein VP2. *Embo J.* **1994**, *13*, 2247–2256. [[CrossRef](#)]
27. Phillips, J.; Braun, R.; Wang, W.; Gumbart, J.; Tajkhorshid, E.; Villa, E.; Chipot, C.; Skeel, R.; Kale, L.; Schulten, K. Scalable molecular dynamics with NAMD. *J. Comput. Chem.* **2005**, *26*, 1781–1802. [[CrossRef](#)]
28. Ribeiro, J.V.; Bernardi, R.C.; Rudack, T.; Stone, J.E.; Phillips, J.C.; Freddolino, P.L.; Schulten, K. QwikMD-integrative molecular dynamics toolkit for novices and experts. *Sci. Rep.* **2016**, *6*, 26536. [[CrossRef](#)]
29. Humphrey, W.; Dalke, A.; Schulten, K. VMD: Visual molecular dynamics. *J. Mol. Graph.* **1996**, *14*, 33–38. [[CrossRef](#)]
30. Tanner, D.E.; Chan, K.Y.; Phillips, J.C.; Schulten, K. Parallel Generalized Born implicit solvent calculations with NAMD. *J. Chem. Theory Comput.* **2011**, *7*, 3635–3642. [[CrossRef](#)]
31. MacKerell, A.D.; Bashford, D.; Bellott, M.; Dunbrack, R.L.; Evanseck, J.D.; Field, M.J.; Fischer, S.; Gao, J.; Guo, H.; Ha, S.; et al. All-Atom Empirical Potential for Molecular Modeling and Dynamics Studies of Proteins. *J. Phys. Chem. B* **1998**, *102*, 3586–3616. [[CrossRef](#)]
32. Roy, U. Structural characterizations of the fas Receptor and the fas-associated protein with death domain interactions. *Protein J.* **2016**, *35*, 51–60. [[CrossRef](#)]
33. Roy, U. Structural modeling of tumor necrosis factor: A protein of immunological importance. *Biotechnol. Appl. Biochem.* **2017**, *64*, 454–463. [[CrossRef](#)]
34. Roy, U. Role of N501Y Mutation in SARS-CoV-2 Spike Protein Structure. *Preprints* **2021**, 2021060238. [[CrossRef](#)]
35. DSV; Discovery Studio Modeling Environment. *Dassault Systèmes BIOVIA Discovery Studio Modeling Environment*; Dassault Systèmes: San Diego, CA, USA, 2015.
36. Chiou, S.S.; Fan, Y.C.; Crill, W.D.; Chang, R.Y.; Chang, G.J. Mutation analysis of the cross-reactive epitopes of Japanese encephalitis virus envelope glycoprotein. *J. Gen. Virol.* **2012**, *93*, 1185–1192. [[CrossRef](#)]
37. Guex, N.; Peitsch, M.C. SWISS-MODEL and the Swiss-PdbViewer: An environment for comparative protein modeling. *Electrophoresis* **1997**, *18*, 2714–2723. [[CrossRef](#)]
38. Scott, W.R.P.; Hünenberger, P.H.; Tironi, I.G.; Mark, A.E.; Billeter, S.R.; Fennen, J.; Torda, A.E.; Huber, T.; Krüger, P.; van Gunsteren, W.F. The GROMOS Biomolecular Simulation Program Package. *J. Phys. Chem. A* **1999**, *103*, 3596–3607. [[CrossRef](#)]
39. Yuan, S.; Ye, Z.W.; Liang, R.; Tang, K.; Zhang, A.J.; Lu, G.; Ong, C.P.; Man Poon, V.K.; Chan, C.C.; Mok, B.W.; et al. Pathogenicity, transmissibility, and fitness of SARS-CoV-2 Omicron in Syrian hamsters. *Science (N. Y.)* **2022**, *377*, 428–433. [[CrossRef](#)]
40. Hashem, A.M.; Algaissi, A.; Almahboub, S.A.; Alfaleh, M.A.; Abujamel, T.S.; Alamri, S.S.; Alluhaybi, K.A.; Hobani, H.I.; AlHarbi, R.H.; Alsulaiman, R.M.; et al. Early Humoral Response Correlates with Disease Severity and Outcomes in COVID-19 Patients. *Viruses* **2020**, *12*, 1390. [[CrossRef](#)]